Reconstructing the Dynamics of FET Oscillators Using Radial Basis Functions

David M. Walker

Department of Applied Science, College of William and Mary, Williamsburg VA 23187-8795
HP Labs, MS4-AD, 1501 Page Mill Rd, Palo Alto CA 94304-1126

Nicholas B. Tufillaro

HP Labs, MS4-AD, 1501 Page Mill Rd, Palo Alto CA 94304-1126
Department of Applied Science, College of William and Mary, Williamsburg VA 23187-8795

(April 13, 1999)

We present the results of a preliminary investigation of the use of nonlinear reconstructions to the modelling of input–output time series data obtained from a nonlinear circuit. We use radial basis function approximations and the extended Kalman filter is utilised to estimate the model parameters. A circuit model of a GaAs FET oscillator is integrated to generate the time domain data used to study our methods.

I. INTRODUCTION

In this paper we will attempt to reconstruct the dynamics of a nonlinear electric circuit model from data using extended Kalman filtering (EKF) and radial basis function approximations. The problem of reconstructing the dynamics of the nonlinear circuit, to be described shortly, requires the modelling of input–output data. We therefore suggest modifications to exisising nonlinear modelling techniques to account for modelling of input–output data. The work described here is a preliminary investigation of our methods to handle nonlinear systems with inputs and outputs and we thus present the results of various approaches whether good or bad.

The outline of this paper is as follows. In Section 2 we introduce concepts from nonlinear dynamics which are useful for reconstructing models from time series. The functions we use to reconstruct the dynamics of the example circuit are radial basis functions, and so we describe these functions in this section. The tool we use in the following to estimate the parameters of our models is the extended Kalman filter. We do not derive the EKF, instead we quote the final algorithm and explain how it can be used for parameter estimation in Section 3. In Section 4 we introduce the nonlinear circuit under consideration. (We derive the governing equations in the Appendix.) We choose a nonlinear circuit to test and develop our methods since nonlinear circuits model real physical devices and so our methods can ultimately be tested experimentally. In Section 5 we reconstruct the dynamics of the nonlinear circuit from output data obtained by integrating the circuit model equations. We reconstruct the dynamics for the case of zero driving, i.e., no inputs, and for the case of non-zero driving. We introduce a new class of models from those previously studied which attempts to reconstruct the dynamics using input–output data. Finally we discuss the results in a concluding section.

II. RECONSTRUCTION OF TIME SERIES

In this paper we report the results of a preliminary investigation involving the nonlinear modelling of input–output time series data for the purposes of short–term prediction, simulation and ultimately characterisation of nonlinear devices. (These are quite lofty goals but we will be satisfied with models that can be simulated for a reasonable length of time, and this in itself is quite a challenge.)

In the following we assume that we are given a scalar output time series $y(t), t = 1, 2, \ldots, N$ and a scalar input time series $v(t), t = 1, 2, \ldots, N$. (The methods we present are easily extended to deal with vector time series.) We further assume that the output and input time series have been embedded with a time delay embedding with lag s to form an extended reconstructed phase space with vectors

$$
\begin{aligned}
z(t) &= [x(t), u(t)] \\
&= [y(t), y(t-s), \ldots, y(t-(k-1)s), \\
&\quad v(t), v(t-s), \ldots, v(t-(l-1)s)].
\end{aligned}
$$

The paper of Casdagli [1] says this is a sensible way of dealing with input–output data. We have proposed a diagnostic to determine the embedding parameters k and l [2]. Rhodes and Morari [3] and Cao et al. [4] have also developed diagnostics for finding suitable embedding dimensions. In the above we have assumed that the inputs are embedded with the same lag as the outputs although this is not necessary. The output lag can be found by standard methods such as choosing the first minimum of the average mutual information function [5,6]. As yet we have not developed a diagnostic which can find an alternative lag for the inputs and so we use the same embedding lag that is used for the outputs.

Our aim is to find a functional relationship (possibly nonlinear) so that

1

$$y(t + 1) = F[z(t)]$$
$$= F[x(t), u(t)].$$

The functional relationship we study in this letter is a radial basis function model. A radial basis function approximation is given by

$$y(t + 1) = \sum_{i=1}^{M} \omega_i \phi(r_i),$$

where $r_i = \|c_i - z_t\|$. The ω_i are called the weights and the c_i are called the centres. The function ϕ is the basis function, and common choices for ϕ include Gaussian functions and cubic functions. The basis functions we will use here are Gaussian functions:

$$\phi(r) = \exp(-\frac{1}{2} r' \Sigma^{-1} r)$$

Another function which may prove useful from an engineering point of view is what we refer to as "Coshy" functions given by

$$\phi(r) = \frac{1}{1 + \cosh(-\sigma r)}.$$

We note that the "Coshy" functions can be readily realised on a silicon chip using a simple analog circuit consisting of a differential amplifier followed by an analog multiplier with bipolar transistors [7]. This suggests that a hardware implementation of radial basis behavioural models can be built into a "product". The Gaussian function is not so tractable. Despite the possibilities of using "Coshy" function models we present our results using Gaussian functions. (The results using "Coshy" functions should be similar and may even be better. This is a topic of future research.)

Radial basis functions are global function approximations with local features due to the location of the centres. The parameters to be estimated in a radial basis approximation are the weights and the location of the centres. The determination of the values for the weights and the locations of the centres is a nonlinear optimisation problem. However, if the centres are chosen *a priori* we reduce the problem to a least squares approximation to find the weights. The scale parameters Σ can also be estimated.

The other problem of radial basis function approximation is to determine an optimal number of basis functions to use. If too few basis functions are used then important dynamics may not be captured by the model. Too many basis functions, however, can cause the model to overfit the data, i.e., fit the noise as well as the dynamics. Models which overfit the data tend to have poor prediction performance when tested on unseen data sets from the same source. We use the EKF in association with description length ideas to determine a suitable number of centres [8].

It is advantageous to consider affine terms in the radial basis function approximation so that

$$y(t + 1) = \beta + \alpha z(t) + \sum_{i=1}^{M} \omega_i \phi(\|c_i - z(t)\|).$$

III. EXTENDED KALMAN FILTER ALGORITHM

In this section we briefly recall the extended Kalman filter update relations and system model before showing how the algorithm can be used for parameter estimation.

The EKF is a statistical state estimator. Given a sequence of observations $y(t)$, not necessarily scalar, the EKF algorithm returns an estimate for the state $x(t)$ and an associated error matrix. The EKF is applied to system models of the form

$$x(t + 1) = f(x(t)) + \xi(t)$$
$$y(t) = c(x(t)) + \nu(t)$$

where f and c are (possibly) nonlinear functions, $\xi(t)$ and $\nu(t)$ are random variables assumed to have normal distributions $P(\xi(t)) \sim N(0, Q)$ and $P(\nu(t)) \sim N(0, R)$ respectively.

The EKF is derived under the assumption that all distributions are normal without proving prior normality implies posterior normality. (This is true for linear systems but is only approximately true for small-noise nonlinear systems.) It is further assumed that the noise is small enough so that Taylor's theorem can be used to estimate the effects of the noise and consequently the distributions all remain normal to sufficient accuracy.

The EKF update relations are [9]

Prediciton

$$m(t) = f(\mu(t - 1))$$
$$S(t) = Q + A(t - 1)\Sigma(t - 1)A'(t - 1)$$

Correction

$$\Sigma(t) = \left(S(t)^{-1} + C'(t)R^{-1}C(t)\right)^{-1}$$
$$K(t) = \Sigma(t)C'(t)R^{-1}$$
$$\mu(t) = m(t) + K(t)(y(t) - c(m(t)))$$

where $A(t - 1) = (Df)_{\mu(t-1)}$ and $C(t) = (Dc)_{m(t)}$. We have assumed that the state $x(t)$ is a random variable, and the estimate of the distribution of $x(t - 1)$ given information up to time $t - 1$ is normal:

$$P(x(t - 1)|y(1), y(2), \ldots, y(t - 1))$$
$$\sim N(\mu(t - 1), \Sigma(t - 1)).$$

Initially, $P(x(0)) \sim N(\mu(0), \Sigma(0))$. If f and c are linear functions the above update relations constitute the Kalman Filter, and the resulting state estimates are optimal in a mean squared sense.

To see how the EKF can be used in the context of parameter estimation, consider the following one–dimensional example

$$x(t + 1) = ax(t) + \xi(t)$$
$$y(t) = x(t) + \nu(t)$$

with a a known constant. This is one of the simplest examples of state estimation, and the Kalman filter is an optimal state estimator. Now, suppose that a is unknown but still assumed to be constant. We can use the Kalman filter, or more correctly the EKF, to simultaneously estimate the states x and the parameter a. The standard way of doing this is to augment the parameter a with the state vector. The system equations are now

$$
\begin{aligned}
x(t + 1) &= a(t)x(t) + \xi(t) \\
a(t + 1) &= a(t) \\
y(t) &= x(t) + \nu(t)
\end{aligned}
$$

Initially, the parameter a is assumed to be normally distributed with mean $a(0)$ and covariance $P(0)$. Observe that there is no noise term in the equation for the evolution of the parameter. Our reason for not including such a term is the stationarity assumption on the parameter a. In many settings, however, the parameter equation is written as

$$a(t + 1) = a(t) + \eta(t).$$

N. B. Treating the parameter as a state variable makes the system equations nonlinear, and so an EKF is used.

There is another way of tackling the problem of parameter estimation with the EKF. Suppose that the states $x(t)$ are known for each t. We can apply the EKF to the following:

$$
\begin{aligned}
a(t + 1) &= a(t) \\
y(t) &= a(t)x(t) + \nu(t).
\end{aligned}
$$

The states $x(t)$ are known, and it is only the parameter a that requires estimation. The observation function is here being regarded as a regression equation.

The above example illustrates two ways in which the Kalman filter can be used for parameter estimation. The general system models are

Method 1

$$
\begin{aligned}
x(t + 1) &= f(x(t), a(t)) + \xi(t) \\
a(t + 1) &= a(t) \\
y(t) &= c(x(t), a(t)) + \nu(t)
\end{aligned}
$$

Here, simultaneous parameter and state estimation is involved. The second system model is

Method 2

$$
\begin{aligned}
a(t + 1) &= a(t) \\
y(t) &= c(x(t), a(t)) + \nu(t)
\end{aligned}
$$

In this case, the states $x(t)$ are known and treated like control inputs. This latter case seems more readily applicable to our examples involving time–delay coordinates, where we already have the embedded states. In general these embedded states are constructed from noisy scalar data, and so are themselves noise corrupted. That is, the scalar time series is

$$y(t) = \hat{y}(t) + \rho(t)$$

where $\hat{y}(t)$ is the true value but $y(t)$ is observed. From these we construct the time–delay vector $z(t)$, which we assume can be written as

$$z(t) = \hat{z}(t) + \eta(t)$$

where $\hat{z}(t)$ is unknown and is constructed from the unknown clean $\hat{y}(t)$.

Since the known states $x(t)$ are typically "noisy" the latter method which assumes they are clean does not cover the full problem of state and parameter estimation. Whence the proposal of the first method to overcome this noisy state problem.

We shall use the EKF with the set–up of method 2 to perform parameter estimation to assumed function models c, for example, radial basis models. The set-up of method 1 attempts to answer the much harder problem of simultaneous parameter and state estimation and we will not dwell further upon it here.

Since we are only going to consider the system models of method 2, we can simplify the EKF update equations somewhat. The evolution of the conditional mean is $\mu(t + 1) = \mu(t)$ which means that $(Df)_{\mu(t)}$ is an identity matrix. Also the dynamic noise $\xi(t)$ is not present so Q is a zero matrix. Thus the prediction step can be combined with the correction step, and with a little algebra we can rewrite the EKF equations as:

$$
\begin{aligned}
K(t) &= \Sigma(t - 1)C(t)'\left(C(t)\Sigma(t - 1)C(t)' + R\right)^{-1} \\
\mu(t) &= \mu(t - 1) + K(t)(y(t) - c(\mu(t - 1))) \\
\Sigma(t) &= \Sigma(t - 1) - K(t)C(t)\Sigma(t - 1)
\end{aligned}
$$

We will use the EKF algorithm to esimate *all* parameters of a Gaussian radial basis model. The system model is given by

$$
\begin{aligned}
\beta(t + 1) &= \beta(t) \\
\alpha(t + 1) &= \alpha(t) \\
c(t + 1) &= c(t)
\end{aligned}
$$

$$\sigma(t+1) = \sigma(t)$$

$$y(t) = \beta(t) + \alpha(t)z(t) +$$
$$\sum_{i=1}^{M} \omega_i(t)\phi(\|c(t) - z(t)\|) + \nu(t)$$

The EKF algorithm is applied to the above system model.

IV. A NONLINEAR CIRCUIT MODEL

The electric circuit we study is a model circuit for an oscillator. The transistor model used in the model circuit is a simplified version of a nonlinear GaAs FET (*Gallium Arsenide Field Effect Transistor*) model first proposed by Curtice and Ettenberg [10]. The circuit model is similar to the circuit models studied by Huang and Chu [11], and also Liao and York [12]. A circuit diagram of the model circuit is shown in Figure 1.

FIG. 1. A nonlinear circuit model of a GaAs FET oscillator.

The model circuit elements consist of resistors, inductors, and capacitors. Some of these elements have non-linear characteristics, and hence the model circuit is non-linear [13]. The nonlinear elements are the capacitances C_{gd} and C_{gs}, the conductances G_{gd} and G_{gs}, and the current element I_{ds}.

The characteristic of I_{ds} is described by

$$I_{ds} = (a_0 + a_1v_1 + a_2v_1^2 + a_3v_1^3)\tanh(\gamma v_{ds})$$

where

$$v_1 = v_{gs}(1 + \beta(v_{ds0} - v_{ds})),$$

and where v_{ds} is the drain–source voltage, v_{gs} is the gate–source voltage, and the remaining terms are constants determined by engineering measurements and experience. The above model for the characteristic of I_{ds} is known as the Curtice-cubic model and was first described by Curtice and Ettenberg [10].

The nonlinear capacitances are modelled by [14]

$$C_{gd} = C_{gd0}\left(1 - \frac{v_{gd}}{v_{bi}}\right)^{-\frac{1}{2}}$$
$$C_{gs} = C_{gs0}\left(1 - \frac{v_{gs}}{v_{bi}}\right)^{-\frac{1}{2}}.$$

v_{gd} is the gate-drain voltage and the remaining undefined terms are constants.

The nonlinear conductances are modelled by

$$G_{gd} = \frac{I_s}{v_{gd}}\left(\exp\left(\frac{v_{gd}}{v_{nt}}\right) - 1\right)$$
$$G_{gs} = \frac{I_s}{v_{gs}}\left(\exp\left(\frac{v_{gs}}{v_{nt}}\right) - 1\right).$$

The new terms I_s and v_{nt} are constants, and also determined by engineering practice.

The linear elements have characteristics described by

Resistor:
$$v = Ri$$

Inductor:
$$v = L\frac{di}{dt}$$

Capacitor:
$$v = \frac{1}{C}\int i \, dt$$

The dynamic behaviour of the circuit can be investigated by studying the circuit equations derived from Kirchoff's Laws. A detailed derivation of the circuit equations for the circuit of Figure 1 is presented in the Appendix.

Using the parameter values specified in the Appendix the nonlinear circuit exhibits self–oscillations under zero driving for certain values of the drain-voltage as we can see from the bifurcation diagram shown in Figure 2. This suggests that a Hopf bifurcation occurs for some value of v_D between 0.6 and 0.8 volts. The bifurcation diagram was obtained by "brute-force". That is, we integrate the dynamical system for a particular value of v_D for a long time to ensure transients have diminished and record the values of the state after this time. We integrated the dynamical system using a variable step size Runge-Kutta solver – Matlab's `ode23` routine. After the initial transient we output the state of the system every 1.0 time steps.
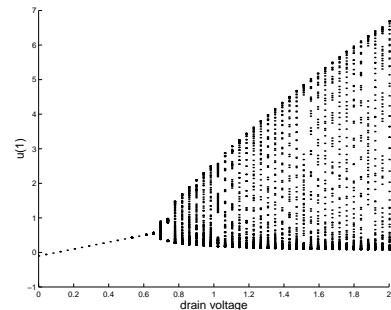
FIG. 2. A bifurcation diagram of the nonlinear circuit equations using the drain-voltage v_D as a bifurcation parameter value. We see that for certain values of v_D the circuit exhibits self–oscillations which suggest that a Hopf bifurcation has occured.

Initially, we attempt to reconstruct the dynamics of the circuit model from three data sets. The first data set is obtained by integrating the dynamical system under zero driving, i.e., $\nu_{ac} = \dot{\nu}_{ac} = 0$, when $v_D = 1.0V$. At this parameter value the dynamical system exhibits self–oscillations. We integrate the dynamical system from time zero to time 200 with sampling time 0.01 time units. The initial condition was $u_i = 0$, $i = 1, \ldots, 6$. We observe the u_3 coordinate. This generates $20,000$ data points and we retain the last $10,000$ points to ensure transients have diminished. A 500 point section of the time series is shown in Figure 3(a). We refer to this data set as the zero drive data set.

The dominant period in the above data is approximately 80 data points, i.e., $T = 0.8$ time units. If we drive the dynamical system with sinusoidal driving at frequency approximately $\frac{2\pi}{T} \approx 7.85 s^{-1}$ we can generate resonant data. The second data set is obtained by integrating the dynamical system as before but we include a sinusoidal driving term of $\nu_{ac} = \sin(7.85t)V$. We refer to this data set as the fast drive data set. A 500 point section of the u_3 time series is shown in Figure 3(b).

The third data set we generate is a slow drive data set. This data set is obtained by integrating the dynamical system with $v_D = 1.0V$ and a driving term of $\nu_{ac} = \sin(0.785t)V$. A $3,000$ point section of the u_3 time series of this slow drive data set is shown in Figure 3(c).
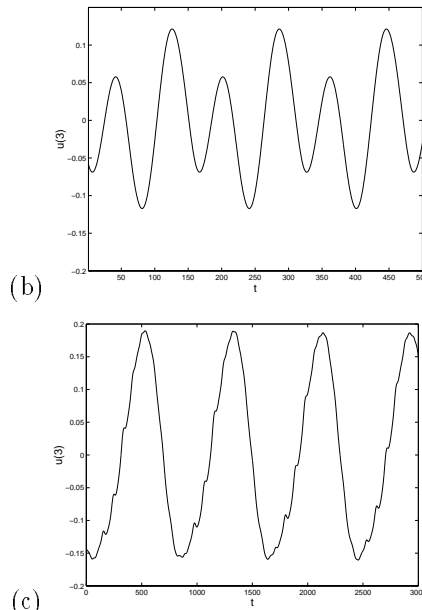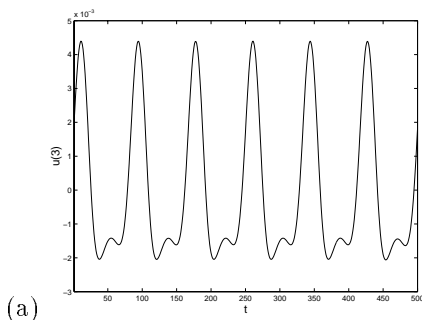
(b)

(c)

FIG. 3. (a) A section of the zero drive data set. (b) A section of the fast drive data set. (c) A section of the slow drive data set.

In nonlinear modelling it is important to reconstruct an appropriate phase space in which to study the data. As mentioned above we will use a time delay embedding of the input and output time series data.

Analysing the zero drive data set by locating the first zero of the linear autocorrelation function we find that embedding the data with a lag of 18 is appropriate. We use this lag for the fast drive data set and the slow drive data set.

Using the method of false nearest neighbours [6] on the zero drive data set with a lag of 18 we find that an embedding dimension of 4 is suggested. We embed the fast drive and slow drive data sets with this embedding dimension.

We note that we have not considered the question of how many past inputs and corresponding lags should be used? We discuss our choices in the next section.

V. EKF RESULTS

In this section we will present the results of our attempts at reconstructing the dynamics of the model circuit using output and input–ouput data.

A. Models from output data

We attempt to reconstruct the dynamics of the model circuit using the zero drive output data, the fast drive output data, and the slow drive output data. That is, we do not use any knowledge of the input data. The

(a)

5

purpose of this exercise is to demonstrate that the non-linear dynamics of the circuit can be reconstructed from data, and so it is appropriate to apply our methods to this problem.

As mentioned above we use the EKF algorithm in the guise of method 2 to reconstruct the dynamics from the zero drive data set. We assume that the dynamics can be adequately reconstructed using a radial basis function model with Gaussian basis functions. We estimate all parameters of the model, i.e., the constant, linear and nonlinear weights, plus the location of the centres and the Gaussian scales. In Figure 4(a)–(b) we show a plot of the Schwarz criterion and description length respectively [8] to give a guide to the number of basis functions to use. Examining these figures we choose to reconstruct the dynamics with 20 basis functions. We also reconstruct the dynamics of the fast and slow drive data sets using 20 basis functions.
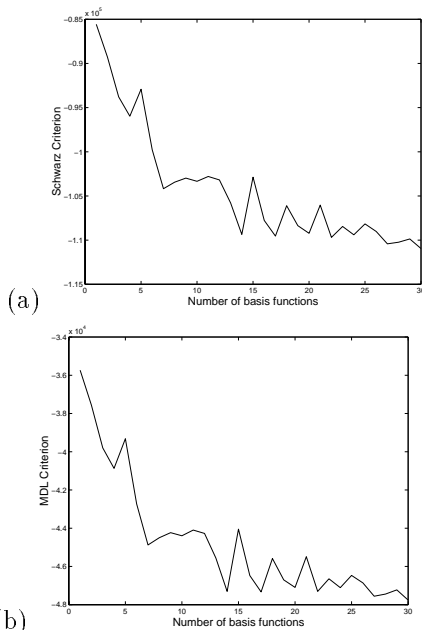
(a)

(b)

FIG. 4. (a) The Schwarz Criterion for increasing number of centres. (b) The MDL Criterion for increasing model size.

We use the first $5,000$ points of the data set to estimate the parameters of the models, and we use the second half (the final $5,000$ data points) of the data set to perform an error test. We only cycle through the training data once.

The modelling errors of the model reconstructed from the zero drive data set were $RMS = 1.6158 \times 10^{-5}$. The test error was $RMS = 1.5827 \times 10^{-5}$. In Figure 5(a) we show a 500 point section of a (noise–free) simulation of the model. The appropriate section of the data is also shown on the figure. We see that the simulation follows

the original time series very well.

We repeat the above process for the fast and slow drive data sets. The modelling errors of the model reconstructed using the fast drive data set were $RMS = 1.7979 \times 10^{-4}$, and the test error was $RMS = 1.8009 \times 10^{-4}$. A 500 point section of a simulation of the model is shown in Figure 5(b). We see once again that the simulation follows the original data very well.

The modelling and test errors for the slow drive data set were $RMS = 3.6342 \times 10^{-4}$ and $RMS = 3.741 \times 10^{-4}$ respectively. A simulated time series is shown in Figure 5(c). In this case, however, we see that the simulated time series is not representative of the original data. This suggests that more care should be taken in choosing the reconstruction parameters, e.g., the time delay, embedding dimension, number of basis functions etc. Indeed, by examining the first zero of the linear autocorrelation for the slow data set a lag of 200 is suggested rather than the lag of 18 we used. Nevertheless, even with this inappropriate choice of time delay we have achieved satisfactory one–step prediction errors.
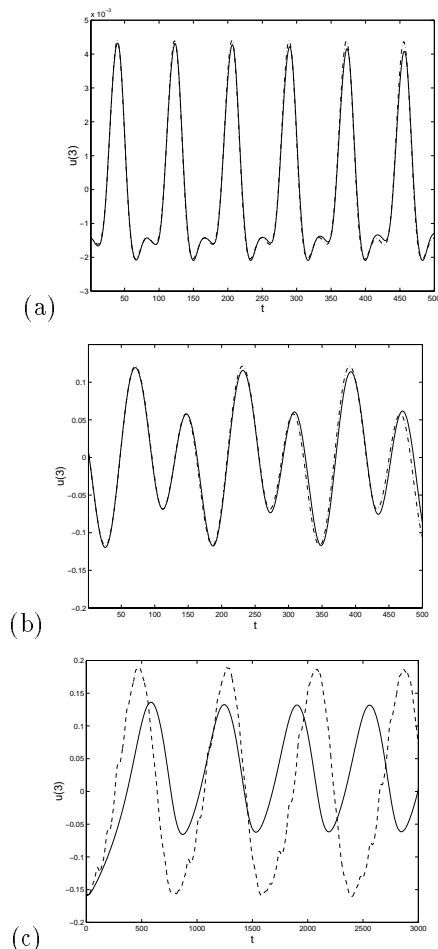
(a)

(b)

(c)

6

FIG. 5. (a) A section of the simulated data and the zero drive data set. (b) A section of the simulated data and the fast drive data set. (c) A section of the simulated data and the slow drive data set. The simulated data is represented by the solid line and the original data by the dashed line.

We have demonstrated that the dynamics of a nonliner circuit model subject to different drives can be reconstructed satisfactorally using radial basis function models. The parameters of the nonlinear model were estimated from output data alone, and no information about the input data was used. This is fine, however, a new model of the dynamics had to be reconstructed for each drive. We would like to use one model for all drives. We try to address this problem in the next two sections. The failure of the simulated orbit of the slow drive model also suggests that it would be beneficial to reconstruct the dynamics by taking into account the inputs.

B. Output data models and input data

As a first attempt to reconstruct the dynamics of the circuit using the fast drive input–output data we consider an additive drive term to the model reconstructed using the zero drive output data. That is, we assume the time series can be modelled by

$$y_{t+1} = f_0(x_t) + L(\hat{u}_t), \qquad (1)$$

where y_t is the output data, x_t is the reconstructed output time series, and $\hat{u}_t$ is the reconstructed input time series. f_0 is the radial basis model reconstructed using the zero drive time series. $L(\hat{u}_t)$ is a linear model of the input time series u_t. The states $\hat{u}_t$ are reconstructed using the same embedding strategies used to reconstruct the states x_t from the output time series y_t.

We have chosen to use the same embedding strategy to embed the inputs as we used to embed the output time series. We know that reconstructing the correct phase space is important, i.e., the choice of the embedding dimension and the time delay is very important for accurate reconstruction of the dynamics. The same should be true for the inputs. Indeed extensions to methods such as false nearest neighbours have been proposed to determine the number of past inputs to use and what the appropriate time delay should be [3,4,2].

As mentioned above we shall use the same embedding strategy to embed the inputs as we used to reconstruct the states from the output data. We bear in mind, however, that improvements to our results may be possible by utilising another embedding strategy.

We have also chosen to reconstruct a linear model for the effect of the inputs. A nonlinear model such as a radial basis function can also be considered.

Examining the differential equation (3) we see that the drives are additive and of the form

$$u(t) = \frac{1}{C_A R_A} \dot{\nu}_{ac}.$$

For the fast drive data,

$$u(t) = \frac{7.85}{C_A R_A} \cos(7.85t),$$

and for the slow drive data set

$$u(t) = \frac{0.785}{C_A R_A} \cos(0.785t),$$

where t is sampled every 0.01 time units starting from 0.0. These are the inputs we use to form the reconstructed inputs $\hat{u}_t$.

We use the EKF algorithm of method 2 to estimate the parameters of $L(\hat{u}_t)$. The EKF system model is

$$a_{t+1} = a_t$$
$$y_t = f_0(x_t) + \sum_{i=0}^{k-1} a_{ti} u_{t-i\tau} + \nu_t.$$

In the above, x_t, u_t, y_t, and f_0 are known and available. The term ν_t represents Gaussian noise with zero mean and covariance R. τ is the time delay and k is the embedding dimension.

We will use the first half of the fast drive data set to estimate the parameters a_i. Using the reconstructed fast drive states and assuming zero inputs the initial fit of (1) had an error of $RMS = 0.005$ and the test error was $RMS = 0.005$. After estimating the a_i parameters using the fast drive inputs we find the fitting errors to be $RMS = 0.001$ and the test error to be $RMS = 0.001$.

As a second test we investigate how the reconstructed model (1) generalises to a different drive. Testing the model using the parameters a_i estimated above on the slow drive data set and the slow drive inputs we find an error of $RMS = 0.0009$. The error assuming zero inputs is $RMS = 0.001$. This demonstrates that the input model of (1) is suitable for short–term prediction of input–output data and models reconstructed using one type of drive can be used for accurate prediction of data produced by a different drive. Unfortunately, the simulated (driven) orbits of (1) do not produce similar time series to those produced by driving the nonlinear circuit equations and so a different approach is called for.

C. Models from input–output data

We have been able to reconstruct the dynamics of the circuit under zero driving. A real physical circuit is nearly always subject to driving. That is, under normal operating conditions the circuit is subject to input forcing, and so the data to reconstruct the zero drive dynamics is not available.

Therefore, the approach followed in the previous section is not apt. It may be possible to use, say, the fast drive data as a new reference for the zero drive dynamics and proceed as above. We shall not develop this idea further here. Instead we shall attempt to reconstruct the dynamics using input–output data at the same time.

The most obvious approach to follow is to append the reconstructed output and input data to form new reconstructed states. That is, the appended state is

$$z_t = [x_t \ \hat{u}_t],$$

where x_t are the reconstructed output states and $\hat{u}_t$ are the reconstructed input states.

We shall reconstruct the dynamics using a radial basis function approximation, so that,

$$y_{t+1} = \beta + \alpha z_t + \sum_{i=1}^{m} \omega_i \phi(r_{ti}), \qquad (2)$$

where $r_{ti} = \|c_i - z_t\|$. We use the EKF algorithm to estimate all parameters.

The data we use is the fast drive data set. We use the first half of the data to estimate the parameters of the model, and keep the second half for a test set. We use the same embedding dimension and time delay as before and reconstruct a model with 20 basis functions. The embedding strategy for the outputs is the strategy used to embed the inputs. The modelling errors for the model were $RMS = 3.869 \times 10^{-4}$ and the test errors were $RMS = 3.866 \times 10^{-4}$.

A simulated (driven) orbit of the above model is shown in Figure 6. We see that after an initial transient the simulation begins to track the data but soon after settles to a periodic orbit with period similar to the data but not amplitude.
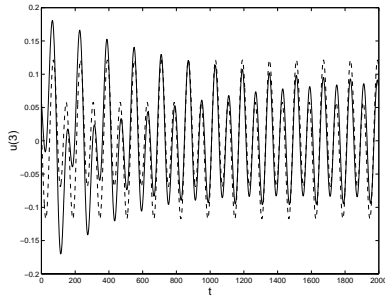

FIG. 6. A simulated (driven) orbit of the nonlinear radial basis model reconstructed using the input–output data of the fast drive data set. The original output data is the dashed line and the simulated orbit is the solid line. We see that after an initial transient the simulated orbit has the same phase as the original data but the amplitudes do not match.

The model can be used for one–step ahead predictions on the slow drive data set, and reasonable performance is observed. Driving the model with the slow drive inputs, however, we do not produce a simulation representative of the slow drive data sets.

D. Models from input–output data measured at the nodes

In the previous sections we have regarded the nonlinear circuit model as a dynamical system described by the differential equation of (3). In so doing, we were able to read–off from the differential equation what the inputs were, and obtain the output data by numerically integrating the differential equation. The output data was simply taken to be one of the solution coordinates of the state of the dynamical system. That is, the system was easily decomposed into a drive system and a response system. The drive system was independent of the response system.

In a test and measurement situation, however, it is the node voltages which are measured. Referring to the circuit diagram of Figure 1 we would measure the voltage at node 4 and consider these as the inputs. The outputs would be obtained by measuring the voltage at, for example, node 2. That is, the input time series would be a sequence of measurements of $e_4 = u_3 + v_S$, and the output time series would be a sequence of measurements of $e_2 = u_1 + u_3 + v_S$.

We observe that these time series are obtained by integrating the differential equation (3). Since the source–load (drive) is a part of the nonlinear circuit there is a feedback coupling between the drive and the response system. That is, the drives are not independent of the responses. There is thus a subtle issue as to what the inputs actually are for the test and measurement of nonlinear devices.

In this section we will reconstruct the dynamics of the circuit given the input–output time series obtained by making measurements at the nodes 2 and 4. The output time series is the voltage at node 2, i.e., e_2, and the input time series is the voltage at node 4, i.e., e_4. We study both fast and slow ν_{ac} driving as before. Figures 7(a)–(b) show sections of the fast and slow drive data sets respectively. In both figures the output time series is the dashed line and the input time series is the solid line.
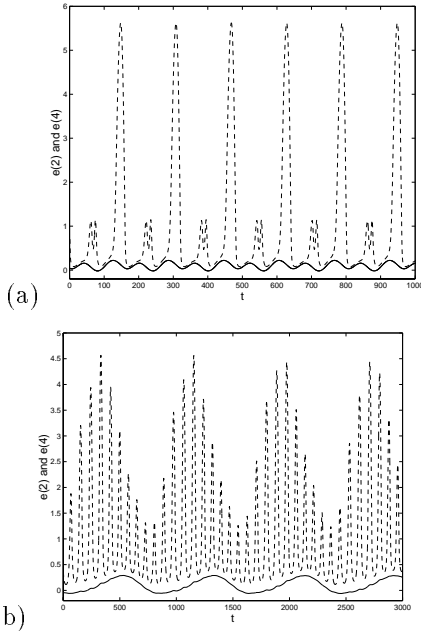
(a)

(b)

FIG. 7. (a) A section of the fast drive node voltage data sets. (b) A section of the slow drive node voltage data sets. The solid line represents the voltage at node 4 (input) and the dashed line represents the voltage at node 2 (output).

We will attempt to reconstruct the dynamics by using radial basis input–output models described by (2). We will use a lag of 18. In Figure 8 we show the results of a false strands calculation applied to the output time series data. An embedding dimension of four is suggested. The embedding strategy used for the input data will be the same as used for the output data. For comparison we show in Figure 9 the results of applying the diagnostic we developed as an extension to the Wayland scheme [15] for detecting determinism to determine appropriate input–output embedding dimensions [2]. The lag we used in this case was 44 obtained by estimating the first minimum of the average mutual information function. We see that the outputs should be embedded in four or five dimensions and two or three past inputs should be used.
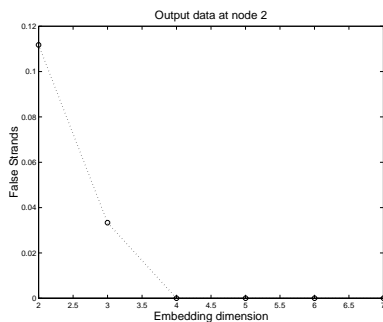

FIG. 8. A false strands calculation applied to the output time series embedded using a lag of 18. We see that embedding with an embedding dimension of four is appropriate.
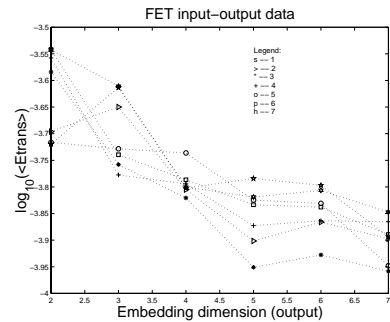

FIG. 9. A plot showing the results of our input-output diagnostic. The outputs should be embedded in four or five dimensions and two or three past inputs should be used. The lag used in the calculation was 44, chosen as an estimate to the first minimum of the average mutual information function.

We fit a radial basis model with 20 Gaussian basis functions. The EKF algorithm is used to estimate the parameters. The modelling and test errors of the model reconstructed using the fast drive node voltage data were $RMS = 0.0546$ and $RMS = 0.0544$ respectively. The model and test errors of the model reconstructed using the slow drive node voltage data were $RMS = 0.0273$ and $RMS = 0.0272$ respectively. Figure 10(a)–(b) shows (driven) simulations of the fast and slow drive models respectively. Once again we see that despite reconstructing a model with good one–step ahead predictions the simulations do not fully capture the behaviour of the original data. For the slow drive simulation, however, some features of the original data are apparent.
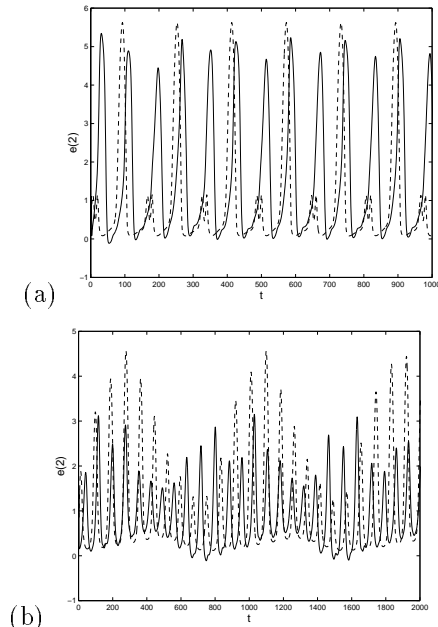

(a)

(b)

FIG. 10. (a) A simulated (driven) orbit of the nonlinear radial basis model reconstructed using the node voltage data of the fast drive data set. (b) A simulated (driven) orbit of the radial basis model reconstructed using the node voltage data of the slow drive data set. The original output data is the dashed line and the simulated orbit is the solid line.

VI. SUMMARY

We have demonstrated that the dynamics of a nonlinear circuit model can be reconstructed from output data and input–output data. We studied the model under different driving conditions to produce three data sets: a zero drive data set, a fast drive data set and a slow drive data set. We found that models with excellent short–term prediction performance and good long–term simulations could be reconstructed using output data alone, although the simulation of the slow drive model was not very good.

We also suggested two methods of reconstructing the dynamics using input–output data. The first method is applicable when the dynamics can be reconstructed from data under zero driving conditions. The model consisted of a radial basis model describing the zero drive dynamics and a linear model of the inputs. (A nonlinear model of the inputs can also be considered.) We found that although accurate short–term prediction could be achieved with this approach, long–term simulations produced time series which were not representative of the data.

The second approach to nonlinear modelling of input–output data was to reconstruct an appended state consisting of the reconstructed output states and the reconstructed input states. We used these appended states in a radial basis function model to model the output time series data. We found that the method was effective in producing models with accurate short–term prediction, and the simulated time series of the models were more representative of the original data than the simulations of the models produced by the first method of input–output modelling.

The above methods demonstrated that the dynamics of the nonlinear circuit can be reconstructed using data, but further study is required in order to be able to use the reconstructed models for simulation. The question of how the dynamics reconstructed by a model using data from one particular drive signal is representative of the dynamics produced by the circuit subject to different driving also needs to be addressed.

We also pointed out that in a real test and measurement process for electrical devices the response circuit and the drive circuit are feedback coupled. This raises the subtle question of what the inputs really are. Since the voltages of the nonlinear circuit can only be measured at certain points (the nodes) we considered the node voltages as input and output time series. For the particular nonlinear circuit under study (Figure 1) we chose the voltage at node 4 as the input and the voltage at node 2 as the output. We demonstrated that accurate short–term prediction was achievable using nonlinear models reconstructed from input–output data. We saw once again that long term simulation of the models did not produce time series representative of the data, although some features were reconstructed.

APPENDIX

The derivation of the circuit equations for the circuit model shown in Figure 1 requires the construction of a circuit graph [16]. A circuit graph for the circuit diagram of Figure 1 is shown in Figure 11.
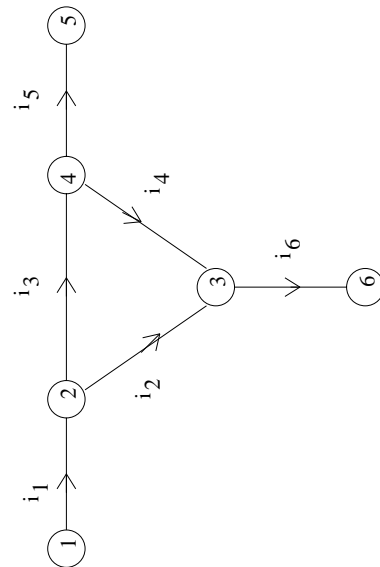

FIG. 11. The circuit graph for the nonlinear circuit model.

If we denote the voltage at node i to be e_i, and choose node 6 as the datum-node so that $e_6 = 0$, Kirchoff's current law at nodes 2, 3, and 4 give the following system of equations.

$$-i_1 + i_2 + i_3 = 0$$
$$-i_2 - i_4 + i_6 = 0$$
$$-i_3 + i_4 + i_5 = 0$$

Substituting for the currents using the characteristics of the elements, and making the change of variables $\{u_1 = e_2 - e_4, u_2 = e_3 - e_4, u_3 = e_4 - v_S\}$ we find that the system becomes

$$-\frac{1}{L_1} \int (v_D - u_1 - u_3 - v_S)dt + C_{gd}(\dot{u}_1 - \dot{u}_2) +$$

$$G_{gd}(u_1 - u_2) + I_{ds} + C_{ds}\dot{u}_1 = 0$$

$$-C_{gd}(\dot{u}_1 - \dot{u}_2) - G_{gd}(u_1 - u_2) + C_{gs}\dot{u}_2 +$$
$$G_{gs}u_2 + \frac{1}{L_2}\int(u_2 + u_3 + v_S)dt = 0$$
$$-I_{ds} - C_{ds}\dot{u}_2 - G_{gs}u_2 + \frac{1}{L_A}\int u_3 dt +$$
$$C_A\dot{u}_3 + \frac{u_3 - \nu_{ac}}{R_A} = 0$$

Differentiating to remove the integrals, and converting to a first order system we arrive at the following dynamical system

$$
\begin{aligned}
\dot{u}_1 &= u_4 \\
\dot{u}_2 &= u_5 \\
\dot{u}_3 &= u_6 \\
\dot{u}_4 &= \frac{C_{gd}H + (C_{gd}+C_{gs})F}{C_{gd}C_{ds}+C_{gs}C_{gd}+C_{gs}C_{ds}} \\
\dot{u}_5 &= \frac{(C_{gd}+C_{ds})\dot{u}_4 - F}{C_{gd}} \\
\dot{u}_6 &= \frac{1}{C_A}(F + G + H)
\end{aligned}
\tag{3}
$$

where

$$F = -\dot{I}_{ds} - \frac{1}{L_1}(u_1 + u_3 + v_S - v_D) -$$
$$(\dot{C}_{gd} + G_{gd})(u_4 - u_5) - \dot{G}_{gd}(u_1 - u_2)$$
$$G = \dot{I}_{ds} + (\dot{C}_{gs} + G_{gs})u_5 + \dot{G}_{gs}u_5 - \frac{u_6 - \dot{\nu}_{ac}}{R_A} - \frac{u_3}{L_A}$$
$$H = -\frac{1}{L_2}(u_2 + u_3 + v_S) - (\dot{C}_{gd} + G_{gd})(u_5 - u_4) -$$
$$\dot{G}_{gd}(u_2 - u_1) - (\dot{C}_{gs} + G_{gs})u_5 - \dot{G}_{gs}u_2$$

The drain–source, gate–drain, and gate–source voltages are given by $v_{ds} = u_1$, $v_{gd} = u_1 - u_2$, and $v_{gs} = -u_2$ respectively.

For zero driving, i.e., $\nu_{ac} = \dot{\nu}_{ac} = 0$ the above dynamical system has an equilibrium solution at $\{u_1 = v_D - v_S, u_2 = -v_S, u_3 = 0, u_4 = 0, u_5 = 0, u_6 = 0\}$. This equilibrium corresponds to the DC solution of the model circuit.

In order to integrate the above dynamical system we must assign cut–off values to the characteristics of the nonlinear elements. This is necessary since the characteristics are approximations to the characteristics measured for real devices. The approximations are only valid around the normal operating regime of the device, and outside of such a regime the approximation no longer holds. The cut–off's used to integrate the system were

Curtice–cubic model: If $|v_{ds}| > 10^{60}$

$$\dot{I}_{ds} = (a_1 + 2a_2 v_1 + 3a_3 v_1^2)\dot{v}_1 \mathrm{sign}(v_{ds})$$

Capacitances: If $v_{gs} \geq 0.999999 v_{bi}$

$$C_{gs} = 1000 C_{gs0}$$
$$\dot{C}_{gs} = 0.$$

If $v_{gd} \geq 0.999999 v_{bi}$

$$C_{gd} = 1000 C_{gd0}$$
$$\dot{C}_{gd} = 0.$$

Conductances: If $v_{gs} > 10^3$

$$G_{gs} = 10^{60}$$
$$\dot{G}_{gs} = 10^{60}.$$

If $v_{gs} = 0$

$$G_{gs} = \frac{I_s}{v_{nt}}$$
$$\dot{G}_{gs} = \frac{I_s \dot{v}_{gs}}{2 v_{nt}^2}.$$

If $v_{gd} = 0$

$$G_{gd} = \frac{I_s}{v_{nt}}$$
$$\dot{G}_{gd} = \frac{I_s \dot{v}_{gd}}{2 v_{nt}^2}.$$

The parameters of the circuit were set to the following values.

Source:

$$
\begin{aligned}
L_A &= 15 nH \\
R_A &= 50 \Omega \\
C_A &= 0.03 nF \\
v_S &= 0.1 V
\end{aligned}
$$

Gate:

$$L_2 = 25 nH$$

Drain:

$$L_1 = 60 nH$$

Curtice–cubic model:

$$
\begin{aligned}
a_0 &= 0.0563 A \\
a_1 &= 0.1022 AV^{-1} \\
a_2 &= 0.0619 AV^{-2} \\
a_3 &= 0.00383 AV^{-3} \\
\gamma &= 1.63 V^{-1} \\
\beta &= 0.047 \\
V_{ds0} &= 2.72 V
\end{aligned}
$$

Capacitances and Conductances:

$$
\begin{aligned}
C_{ds} &= 0.135 \times 10^{-3} nF \\
C_{gs0} &= 0.45 \times 10^{-3} nF \\
C_{gd0} &= 0.1 \times 10^{-3} nF \\
v_{bi} &= 0.6516 V \\
I_s &= 7.13 \times 10^{-12} A \\
v_{nt} &= 0.03146 V
\end{aligned}
$$

The drain–voltage v_D is unspecified as it is chosen to be a bifurcation parameter ranging from $0V$ to $2V$.

[1] M. Casdagli, *in Nonlinear Modeling and Forecasting*, edited by M. Casdagli and S. Eubank, (Addison-Wesley, Reading, MA, 1992).

[2] D. M. Walker and N. B. Tufillaro, *HP Technical Report*, **HPL-1999-24** 1999.

[3] C. Rhodes and M. Morari, *Proceedings of the American Control Conference*, Seattle, 2190–2195, 1995.

[4] L. Cao, A. Mees, K. Judd and G. Froyland, *Int. J. Bif. Chaos*, **8**(7), 1491, 1998.

[5] A. M. Fraser and H. L. Swinney, *Phys. Rev. A.* **33**, 1134, 1986.

[6] H. D. I. Abarbanel, R. Brown, J. J. Sidorowich and L. S. Tsimring, *Rev. Mod. Phys* **65**, 1331 (1993).

[7] T. Miyano and K. Aihara, *Proceedings of International Symposium on Artificial Life and Robotics*, 150–153, 1997.

[8] D. M. Walker and A. I. Mees, *Int. J. Bif. Chaos.*, **8**(3), 557, 1998.

[9] O. L. R. Jacobs, *Introduction to Control Theory*, (Oxford Science Publications, 1993).

[10] W. R. Curtice and M. Ettenberg, *IEEE Trans. Microwave Theory Tech.*, **MTT–33**, 1383 (1985).

[11] C. C. Huang and T. H. Chu, *IEEE Trans. Microwave Theory Tech.*, **42**, 1851 (1994).

[12] P. Liao and R. A. York, *IEEE Trans. Microwave and Guided Wave Lett.*, **4**, 20 (1994).

[13] M. Hasler and J. Neirynck, *Nonlinear Circuits* (Artech House, 1986).

[14] S. A. Maas, *Nonlinear Microwave Circuits* (IEEE Press, 1986).

[15] R. Wayland, D. Bromley, D. Pickett, and A. Passamente, *Physical Review Letters*, **70**(5), 580, 1993.

[16] L. O. Chua, C. A. Desoer and E. S. Kuh, *Linear and Nonlinear Circuits*, (New York: McGraw–Hill, 1987).